



Error propagation for the Molodensky G_1 term

J. C. McCubbine^{1,3} · W. E. Featherstone^{2,3} · N. J. Brown^{1,3}

Received: 31 January 2018 / Accepted: 23 October 2018 / Published online: 9 November 2018
© The Author(s) 2018

Abstract

Molodensky G terms are used in the computation of the quasigeoid. We derive error propagation formulas that take into account uncertainties in both the free air gravity anomaly and a digital elevation model. These are applied to generate G_1 terms and their errors on a $1'' \times 1''$ grid over Australia. We use these to produce Molodensky gravity anomaly and accompanying uncertainty grids. These uncertainties have average value of 2 mGal with maximum of 54 mGal. We further calculate a gravimetric quasigeoid model by the remove–compute–restore technique. These Molodensky gravity anomaly uncertainties lead to quasigeoid uncertainties with a mean of 4 mm and maximum of 80 mm when propagated through a deterministically modified Stokes’s integral over an integration cap radius of 0.5° .

Keywords Quasigeoid · Molodensky theory · G_1 term · Height anomaly · Error propagation

1 Introduction

The height anomaly is required if one wishes to transform GNSS-derived ellipsoidal heights to normal heights and vice versa. Height anomalies are the separation between the telluroid and the Earth’s surface or, equivalently, the separation between a geocentric reference ellipsoid and the quasigeoid (e.g. Moritz 2015). Their values come from the solution to Molodensky boundary-value problem (Molodensky et al. 1960, 1962; Heiskanen and Moritz 1967) and can be determined by evaluating Stokes’s integral with the Molodensky gravity anomaly in place of the classical gravity anomaly used to calculate the geoid (e.g. Vaníček 1974).

Molodensky problem has been studied quite extensively from the theoretical point of view (e.g. Pellinen 1962; Brovar 1964; Sansó 1978, 1989; Costea et al. 2014; Foroughi and Tenzer 2014; Banz et al. 2014, among others). The Molodensky free air gravity anomaly is gravity acceleration at the

Earth’s surface minus normal gravity at the corresponding point on the telluroid. The gravitational effects of the topography can be expressed as an infinite power series of so-called G terms, derived from convolution integrals of Molodensky free air gravity anomalies and normal heights (e.g. Moritz 1970). These are added to the Molodensky free air anomaly to give what we abbreviate in the following as the Molodensky gravity anomaly. For regional quasigeoid computations, this power series is typically truncated to the first order (e.g. Burša 1965; Rapp 1975; Amod and Merry 2002, Merry 2003) to the so-called G_1 term, though higher-order G terms have also been considered (e.g. Sideris and Schwarz 1988; Li et al. 1995; Denker and Tziavos 1999).

The most recent gravimetric quasigeoid model of Australia, AGQG2017 (Featherstone et al. 2018a, b) was computed using Faye gravity anomalies (e.g. Moritz 1968) as an approximation of Molodensky gravity anomalies (cf. Amod and Merry 2002; Mojzeš et al. 2005). Faye gravity anomalies are calculated by adding the planar gravimetric terrain correction to the free air anomaly as an approximation of the G_1 term, but the terrain correction is always positive, whereas the G_1 term can take both positive and negative values due to the inclusion of the free air anomaly. This approximation will be investigated herein.

McCubbine et al. (2017) provide a mathematical framework to compute planar gravimetric terrain correction uncertainties. The presentation here provides a similar methodology to determine first-order Molodensky gravity anomaly

✉ J. C. McCubbine
jack.mccubbine@ga.gov.au

¹ Geodesy Section, Community Safety and Earth Monitoring Division, Geoscience Australia, GPO Box 378, Canberra, ACT 2601, Australia

² School of Earth and Planetary Sciences, Curtin University of Technology, GPO Box U1987, Perth, WA 6845, Australia

³ Cooperative Research Centre for Spatial Information for This Project, Level 5, 204 Lygon Street, Carlton, VIC 3053, Australia

uncertainties based on the assumption that the DEM and free air anomaly errors are zero-mean Gaussian random variables that are spatially independent. This work closes a gap in the existing literature on an error propagation formula. This is extended further to determine the error in the computed quasigeoid (cf. Featherstone et al. 2018a).

We present the computation of G_1 terms and their errors on a $1'' \times 1''$ grid over Australia and $1' \times 1'$ grids of quasigeoid heights and their errors, computed using the remove–compute–restore technique with the Featherstone et al. (1998) modified Stokes’s kernel. Here, the computational procedures for the quasigeoid heights are performed deterministically, with the propagated error computations treated completely separately. As such, the propagated errors have no effect on the computed quasigeoid itself.

2 First-order solution to the Molodensky problem

The height anomaly ζ can be determined by evaluating Stokes’s integration of Molodensky free air anomalies and an infinite sum of Molodensky G_n terms. The commonly used first-order Stokesian solution is

$$\zeta = \frac{R}{4\pi\gamma} \iint_{\Omega} (\Delta g_{FA} + G_1) S(\Psi) d\Omega \quad (1)$$

where γ is normal gravity on the telluroid (e.g. Denker and Tziavos 1999), Δg_{FA} is the Molodensky free air gravity anomaly on the surface of the topography, $S(\Psi)$ is Stokes’s kernel or some modification thereof, and G_1 is the first-order Molodensky gravity correction term, given by, e.g. Moritz (2015)

$$G_1(\phi, \lambda) = \frac{R^2}{2\pi} \iint \frac{H^*(\phi', \lambda') \Delta g_{FA}(\phi', \lambda')}{l(\phi, \lambda, \phi', \lambda')^3} - \frac{H^*(\phi, \lambda) \Delta g_{FA}(\phi', \lambda')}{l(\phi, \lambda, \phi', \lambda')^3} \cos(\phi') d\phi' d\lambda'. \quad (2)$$

In Eq. (2), H^* is the normal height and $l = 2R\sin(\Psi/2)$ is the distance between the roving point of the integral and each computation point, where R is the mean Earth radius and Ψ is the spherical distance on the unit sphere. When H^* and Δg_{FA} are gridded, the G_1 convolution integral can be discretised and expressed in spectral form as (cf. Sideris and Schwarz 1986, 1988)

$$G_1 = \frac{\Delta\phi\Delta\lambda}{2\pi} \left[(H^* \Delta g_{FA}) * \frac{1}{l^3} - H^* \left(\Delta g_{FA} * \frac{1}{l^3} \right) \right], \quad (3)$$

where $\Delta\phi$ and $\Delta\lambda$ are the latitudinal and longitudinal grid spacings (dimensions of length after discretisation). In the frequency domain, the convolutions become multiplication

(since $f * g = F^{-1}(F(f)F(g))$), which can be efficiently evaluated using the discrete/fast Fourier transform. Wavelet formulations have been proposed by Yu et al. (2001) and Freeden and Mayer (2006), but here we only consider the Fourier case. However, we do make use of the very efficient FFTW algorithm (Frigo and Johnson 2005).

We calculated a $1''$ by $1''$ (~ 30 m resolution) grid of Molodensky G_1 terms over the entire Australian continent. We used the $1'' \times 1''$ digital elevation model (DEM) provided by Geoscience Australia (Gallant et al. 2011) as normal height values and a $1'' \times 1''$ grid of Molodensky free air gravity anomalies interpolated from values in the Geoscience Australia land gravity database. The DEM was derived from Shuttle Radar Topography Mission (SRTM) ellipsoidal heights, converted to physical heights using EGM96 (Lemoine et al. 1998) and “hydrologically enforced” using the ANUDEM software (Hutchinson 1989) to ensure that streams and rivers flow in the correct direction.

Similarly to the planar terrain correction presented by McCubbine et al. (2017), we evaluated the convolution integrals out to a maximum distance of 0.5° (~ 50 km) from the computation point. This was done so that the G_1 terms could be used to compute quasigeoid solutions that are comparable to those in Featherstone et al. (2018a). We also used a kernel weighting function (McCubbine et al. 2017)

$$w = \frac{2l^4}{\left(l + \frac{\Delta l}{2}\right)^2 \left(l - \frac{\Delta l}{2}\right)^2}, \quad (4)$$

to estimate kernel values that are more representative of their mean over each $1'' \times 1''$ cell compared to just the value at each centre. The G_1 term values are shown in Fig. 1, generalised to $1'$ by $1'$ for display purposes. Statistics of the $1'' \times 1''$ grid are given in the caption.

The $1'' \times 1''$ DEM and gravity anomaly grids each occupy approximately 80 Gb in ASCII format. These are too large to be read into core memory on a PC, so they were broken into $5^\circ \times 5^\circ$ sub-grids with a 1° overlaps at each edge. The 1° overlap ensures that the sub-grids agree at the boundaries since the integrals were evaluated out to a maximum 0.5° radius from each computation point. For the EW direction, the agreement was exact because the tiles overlap by more than the integration radius. For the NS direction, the agreement was less than 10^{-4} mGal because the mean latitude of each sub-grid was used to compute the spherical distance. We then computed the G_1 term at each sub-grid element and “stitched” the tiles back together using the GMT (Wessel et al. 2013) routine *grdblend*.

The computations were performed using a Matlab™ script that makes use of highly efficient in-built Fourier transform routines (FFTW; Frigo and Johnson 2005). There were 90 individual DEM and free air anomaly sub-grids in total, and the script took approximately 25 min to run for each tile. The

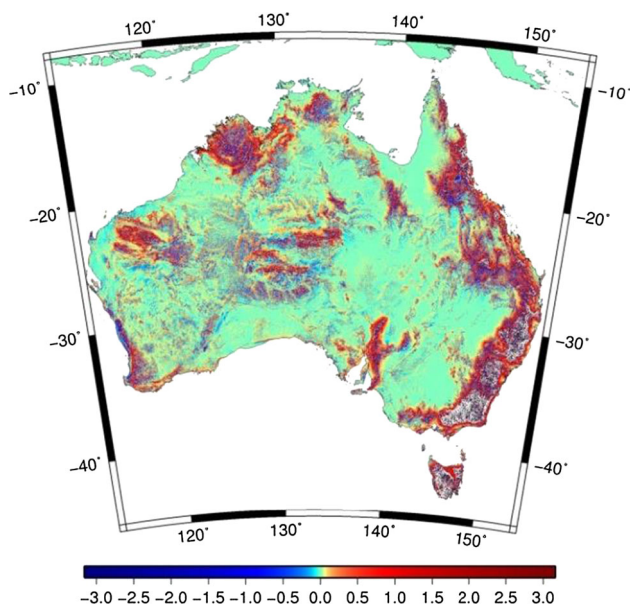


Fig. 1 $1'' \times 1''$ Molodensky G_1 terms block-averaged to a $1' \times 1'$ resolution. For the $1'' \times 1''$ grid: [min: -113.698 , max: 139.588 , mean: 0.037 , STD: 0.998] mGal

total run time to compute the $1'' \times 1''$ resolution G_1 terms was 37.5 h, a testament to the efficiency of the FFTW.

3 Free air anomaly and DEM error propagation into the G_1 term

For the G_1 term error propagation formulas derived in this section, we make the implicit assumption that Eq. (2), and its discretisation given by Eq. (3), do not introduce any error. This is not strictly true, however. For example, Eq. (2) neglects the angle of inclination of the heights between the computation and roving points (Baussus-von Luetzow 1971). Similarly, Eq. (3) discretises the integral so that it is possible to evaluate it numerically, but the topographic heights and gravity field are continuous in reality. However, these equations are widely used and their theoretical deficiencies are well documented elsewhere.

In the following, we consider the propagation of errors in the gravity anomaly data and DEM heights into the G_1 term by looking at the Taylor series expansion of Eq. (3) around these terms. The contribution of a single grid element at (ϕ', λ') to the G_1 term at (ϕ, λ) is given by

$$\begin{aligned}
 G'_1 &= \frac{\Delta\phi\Delta\lambda}{2\pi} \left[\frac{H^*(\phi', \lambda')\Delta g_{FA}(\phi', \lambda')}{1(\phi, \lambda, \phi', \lambda')^3} - \frac{H^*(\phi, \lambda)\Delta g_{FA}(\phi', \lambda')}{1(\phi, \lambda, \phi', \lambda')^3} \right] \\
 &= \frac{\Delta\phi'\Delta\lambda'}{2\pi} \left[\frac{H'^*\Delta g'_{FA}}{l^3} - \frac{H^*\Delta g'_{FA}}{l^3} \right] \tag{5}
 \end{aligned}$$

A small change in the normal height and free air anomaly at the roving point (denoted by dH'^* and $\delta dg'_{FA}$, respectively) and computation point height (denoted δH) on the G'_1 value can be evaluated by considering the Taylor series expansion around these terms, which is

$$\begin{aligned}
 &G'_1(H'^* + dH'^*, H^* + dH^*, \Delta g'_{FA} + d\Delta g'_{FA}) \\
 &\quad - G'_1(H'^*, H^*, \Delta g'_{FA}) \\
 &= \sum_{j=1}^{\infty} \frac{1}{j!} \left(dH'^* \frac{\partial}{\partial H'^*} + dH^* \frac{\partial}{\partial H^*} + d\Delta g'_{FA} \frac{\partial}{\partial \Delta g'_{FA}} \right)^j \\
 &G'_1(H'^*, H^*, \Delta g'_{FA}) \\
 &= \frac{\Delta\phi\Delta\lambda}{2\pi} \left[(dH'^* - dH^*) \frac{\Delta g'_{FA}}{l^3} + (dH'^* - dH^*) \frac{d\Delta g'_{FA}}{l^3} \right. \\
 &\quad \left. + d\Delta g'_{FA} \frac{H'^* - H^*}{l^3} \right] \tag{6}
 \end{aligned}$$

By considering the dH'^*, dH^* and $d\Delta g'_{FA}$ terms as stochastic quantities (uncertainties), we can evaluate the variance of G'_1

$$\begin{aligned}
 Var(G'_1) &= \frac{\Delta\phi^2\Delta\lambda^2}{4\pi^2} \left[\frac{\Delta g'^2_{FA}}{l^6} Var(dH'^* - dH^*) + \frac{1}{l^6} Var \right. \\
 &\quad \left. ((dH'^* - dH^*)d\Delta g'_{FA}) + \frac{(H'^* - H^*)^2}{l^6} Var(d\Delta g'_{FA}) \right. \\
 &\quad + \frac{2\Delta g'_{FA}}{l^6} Cov(dH'^* - dH^*, (dH'^* - dH^*)d\Delta g'_{FA}) \\
 &\quad + \frac{2\Delta g'_{FA}(H'^* - H^*)}{l^6} Cov(dH'^* - dH^*, d\Delta g'_{FA}) \\
 &\quad \left. + \frac{2(H'^* - H^*)}{l^6} Cov((dH'^* - dH^*)d\Delta g'_{FA}, d\Delta g'_{FA}) \right] \tag{7}
 \end{aligned}$$

To simplify Eq. (7), we have made the following three initial assumptions about the DEM and free air gravity anomaly uncertainties:

- (i) dH'^*, dH^* and $d\Delta g'_{FA}$ are zero-mean Gaussian random variables with variances $\sigma^2_{dH'^*}, \sigma^2_{dH^*}$ and $\sigma^2_{d\Delta g'_{FA}}$;
- (ii) $d\Delta g'_{FA}$ and DEM values dH'^* and dH^* values are spatially independent, i.e. no correlation among values in nearby grid cells;
- (iii) $d\Delta g'_{FA}$ are independent to the dH'^* values.

None of these assumptions are strictly true, however. For (i), the exact nature of the gravity anomaly and DEM errors are unknown. In the absence of any concrete information to the contrary, we assume them to be random, non-systematic, and equally likely to fall either side of a zero mean for convenience, which leads to the choice of a Gaussian distribution. For (ii), the errors in the DEM are typically correlated out to approximately 100 m (Gallant et al. 2011) and the gravity data used to determine the $1'' \times 1''$ grid have an Australia-wide average spatial density of around one measurement

every 4 km² (but this varies from place to place: see Fig. 1 in Featherstone et al. 2018a), so neighbouring grid cells may be determined from the same surveys. These effects could be compensated for with additional covariance terms, which, however, are neglected in the following for simplicity (cf. McCubbine et al. 2017). For point (iii), the free air anomalies were determined using a “topographic restoration procedure” (Featherstone and Kirby 2000), which implicitly causes correlated errors between the free air gravity anomalies and DEM; this is addressed in Appendix A, although it drastically increases the complexity of the error variance computation so has not been performed.

Under all the above assumptions, the simplified expression of the $Var(G'_1)$ (Eq. 7) is given by

$$Var(G'_1) \cong \frac{\Delta\phi^2 \Delta\lambda^2}{4\pi^2 16} \left[\Delta g'^2_{FA} (\sigma_{dH^*}^2 + \sigma_{dH'^*}^2) + \sigma_{d\Delta g'_{FA}}^2 (H'^{*2} - 2H'^*H^* + H^{*2}) + \sigma_{d\Delta g'_{FA}}^2 (\sigma_{dH}^2 + \sigma_{dH'}^2) \right]. \tag{8}$$

Following McCubbine et al. (2017), the variance of the G_1 term convolution integral can then be expressed as a sum of convolutions by

$$Var(G_1) = \frac{\Delta\phi^2 \Delta\lambda^2}{4\pi^2} \left[\sigma_{dH^*}^2 \left(\Delta g'^2_{FA} * \frac{1}{16} \right) + \left(\sigma_{dH'^*}^2 \Delta g'^2_{FA} * \frac{1}{16} \right) + \left(\sigma_{d\Delta g'_{FA}}^2 H'^{*2} \right) * \frac{1}{16} - 2H \left(\sigma_{d\Delta g'_{FA}}^2 H'^* * \frac{1}{16} \right) + H^{*2} \left(\sigma_{d\Delta g'_{FA}}^2 * \frac{1}{16} \right) + \sigma_{\delta H^*}^2 \left(\sigma_{d\Delta g'_{FA}}^2 * \frac{1}{16} \right) + \left(\sigma_{dH'^*}^2 \sigma_{d\Delta g'_{FA}}^2 * \frac{1}{16} \right) \right]. \tag{9}$$

We calculated G_1 error variances using Eq. (9) with the 1'' × 1'' DEM, assuming the height errors at each grid point to be independent with a standard deviation of ±7.66 m (cf. McCubbine et al. 2017), a gridded 1'' × 1'' free air anomaly, and a 1'' × 1'' gridded free air anomaly errors used for AGQG2017 (Featherstone et al. 2018a). Equation (9) is valid for spatially varying DEM error standard deviations (i.e. error standard deviation values gridded at the same resolution as the free air anomalies and DEM, rather than a constant value), but these estimates are currently unavailable for the DEM used in this study.

Figure 2 shows the square root of the G_1 uncertainty values re-gridded at 1' × 1' for display purposes; statistics of the 1'' × 1'' grid are given in the caption. The gravity observations used for these calculations have been collected during regional surveys of different extents with varying methodologies and instrumentation. This leads to heterogeneous uncertainties among different survey areas, which results in some spurious linear features at the boundaries in Fig. 2, e.g. at 30°S and 128°E.

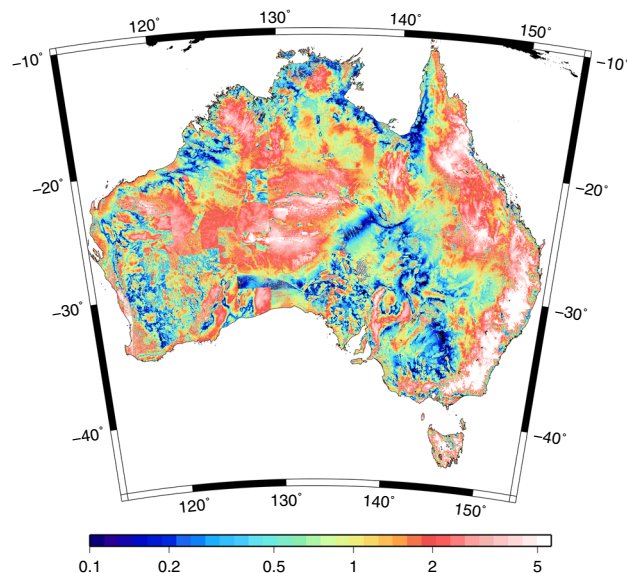


Fig. 2 1'' × 1'' Molodensky G_1 term uncertainty estimates block-averaged to a 1' × 1' resolution. For the 1'' × 1'' grid: [min: 0, max: 43.715, mean: 0.244, STD: 0.805] mGal

Finally, due to the assumptions regarding independence and the fact that the G_1 term integral is zero at the computation point, the variance of the Molodensky gravity anomaly Δg is given by

$$Var(\Delta g) = Var(\Delta g_{FA}) + Var(G_1) \tag{10}$$

The standard deviation (square root of variance) of the Molodensky gravity anomaly $Var(\Delta g)$ is shown in Fig. 3, with the variances of the free air gravity anomalies $Var(\Delta g_{FA})$ taken from Featherstone et al. (2018a). The gridding of the gravity anomaly data also introduces some errors. These are not reflected in the free air anomaly error standard deviation grid here because they are not given by the GMT gridding procedure directly.

4 Quasigeoid determination and error propagation through Stokes’s integral

The Molodensky G_1 term is theoretically superior to the planar terrain correction for computing the height anomaly. We therefore used the G_1 term in place of the planar terrain correction values for a series of regional quasigeoid computations, producing a range of solutions by the remove–compute–restore technique with EGM2008 (Pavlis et al. 2012, 2013) as the reference field and Curtin University’s FFTmod1D2011.f software (Hirt et al. 2011).

We used the Featherstone et al. (1998) modified Stokes’s kernel (herein abbreviated to FEO) with modification degrees ranging from 40° to 120° (in 20° increments) and spherical

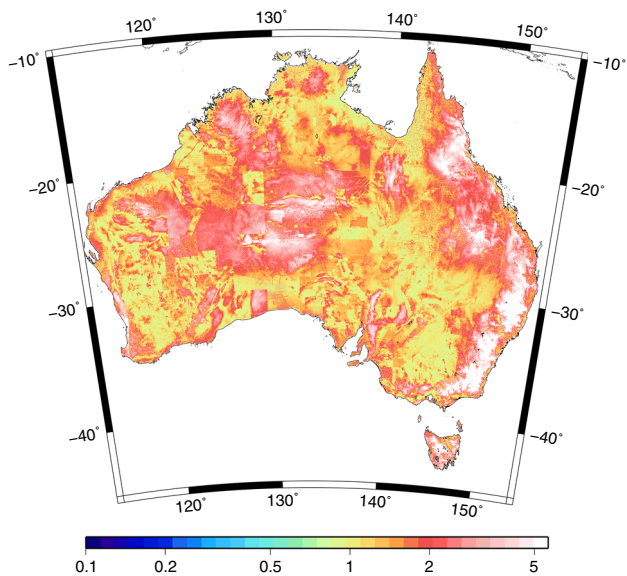


Fig. 3 $1'' \times 1''$ Molodensky gravity anomaly error standard deviations block-averaged to a $1' \times 1'$ resolution. For the $1'' \times 1''$ grid: [min: 0.003, max: 54.201, mean: 2.026, STD: 2.881] mGal

cap radii ranging from 0° to 5° (in 0.5° increments). The FEO kernel modification minimises the L2-norm of the truncation bias and accelerates convergence of the truncation bias per degree by making the error kernel’s derivative continuous at the truncation radius. The quasigeoid solutions were compared to GNSS-levelling data, which are described in Featherstone et al. ((2018a, b)). The standard deviation of the comparisons is shown in Fig. 4. Quasigeoid models produced using planar terrain corrections fit the GNSS-levelling data slightly better for each parameter combination after removal of a plane to account for the predominantly north south tilt in the Australian Height Datum (cf. Featherstone and Filmer 2012).

The modification degree and integration cap radius together act as partial high pass filters on the integrated signal (Vaníček and Featherstone 1998). In Fig. 4, when the integration cap radius is small ($< 1^\circ$), it is the dominant high pass filter. This is evidenced by little difference among the quasigeoid solutions with different modification degrees for both the Faye and Molodensky anomalies. As the integration cap radius increases and the power of the filter thus lessens, long-wavelength errors in the terrestrial gravity data pass more into the quasigeoid solutions. This is more prominent for lower modification degrees, again where the filter is less powerful.

The quasigeoid solution using the G_1 term that best agrees with the GNSS-levelling data is obtained with a modification degree of 40 and an integration cap radius of 0.5° . This is exactly the same parameter combination found for AGQG2017 (Featherstone et al. 2018a). However, as with AGQG2017, these results must be balanced against the inherent ~ 40 mm precision of the GNSS-levelling data (cf.

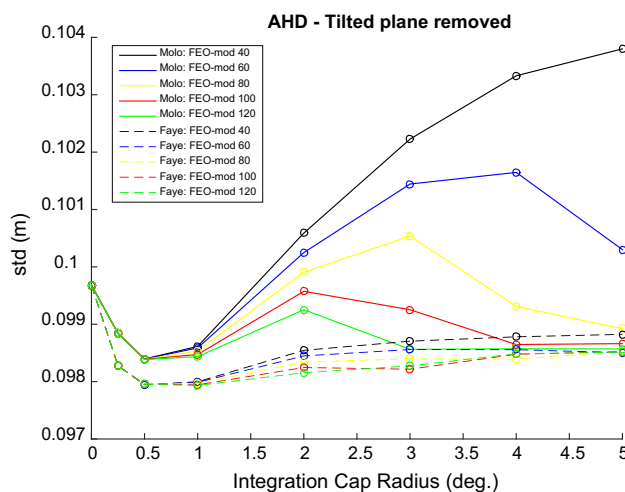


Fig. 4 STD (m) of gravimetric quasigeoid models for parameter sweeps of FEO kernel modification degree and spherical integration cap radius versus GNSS-levelling data after removal of a tilted plane using the G_1 term (solid lines) and the planar terrain correction (dashed lines—from Featherstone et al. 2018a), both determined from $1'' \times 1''$ grids

Featherstone et al. 2018a, Sect. 2.4), which makes any definitive discrimination among the model solutions difficult for the range of the y-axis in Fig. 4.

The quasigeoid solutions using $1'' \times 1''$ planar terrain corrections always agree better (or at least the same) with the GNSS-levelling data than those determined using the $1'' \times 1''$ G_1 terms. We postulate that the slightly weaker agreement of the quasigeoid solutions determined using the G_1 term to the GNSS-levelling data is due to the sparser gravity data coverage in relation to the DEM resolution, i.e. inadequately dense gravity observations used to grid the free air anomaly at $1'' \times 1''$ for the G_1 term computation. This is arguably a limitation of the Molodensky method because it appears to require gravity observations at a spatial density commensurate with the resolution of the DEM used.

To further investigate this postulate, we computed G_1 terms and planar terrain corrections using coarser $1' \times 1'$ grids of free air anomalies and DEM heights, and used these to determine quasigeoids with the same sweeps of Stokes’s integral parameters as shown in Fig. 4. This test revealed that the G_1 terms outperformed the planar terrain corrections in this instance (Fig. 5). Further work should be undertaken to shed more light on this behaviour, however. For example, the resolution of the DEM and gridded free air anomaly data could be varied prior to the computation of planar terrain corrections and G_1 terms to test our postulate.

Gravity anomaly error variances $\sigma^2(\Delta g)$ were propagated through a modified version of Stokes’s integral to produce error estimates of the quasigeoid heights $\sigma^2(\zeta)$. Following the methods in Featherstone et al. (2018a), error variances of regional quasigeoid heights determined by the remove–compute–restore procedure can be approximated using global

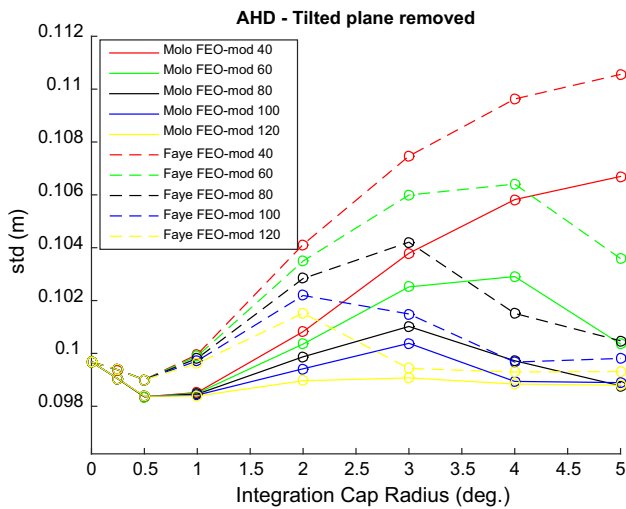


Fig. 5 STD (m) of gravimetric quasigeoid models for parameter sweeps of FEO kernel modification degree and spherical integration cap radius versus GNSS-levelling data after removal of a tilted plane using the G_1 term (solid lines) and the planar terrain corrections, both determined from $1' \times 1'$ grids

gravity model error variance estimates and gravity anomaly error variances by

$$\sigma^2(\zeta_i) = \sigma^2(\zeta_i)_{GGM} + \kappa^2 \sum_{\Omega} \sigma^2(\Delta g_j) \widehat{S}^2(\psi_{i,j}) d\Omega^2 - \kappa^2 \times \sum_{\Omega} \sigma^2(\Delta g_j)_{GGM} \widehat{S}^2(\psi_{i,j}) d\Omega^2 \quad (11)$$

where \widehat{S} is the FEO-modified Stokes’s kernel, $\sigma^2(\zeta_i)_{GGM}$ and $\sigma^2(\Delta g_j)_{GGM}$ are the reference global gravity model quasigeoid height and gravity anomaly error variances, respectively, $\kappa = r/4\pi$ for geocentric radius r , point i is the computation point and point j is the roving point of the integration.

Figure 6a shows the Molodensky gravity anomaly errors supplemented by Sandwell et al. (2013) satellite altimetry gravity anomaly errors offshore. Figure 6b shows their contribution to the quasigeoid height errors (i.e. the second term on the right-hand side of Eq. 11) with the same integration parameters used to generate the quasigeoid model. Figure 6c shows the EGM2008 quasigeoid height error $\sigma(\zeta_i)_{EGM2008}$. Figure 6 (d) shows the final quasigeoid height standard deviation $\sigma(\zeta_i)$ derived via Eq. (11). Both the EGM2008 gravity anomaly and quasigeoid error grids were downloaded from http://earth-info.nga.mil/GandG/wgs84/gravitymod/egm2008/egm08_error.html. These were determined by the EGM2008 development team by propagating error estimates of the raw gravity data used to determine EGM2008 through (an unmodified) Stokes’s integral (Pavlis and Saleh 2005).

The propagated Molodensky gravity anomaly uncertainties produce quasigeoid uncertainties with a mean of 4 mm

and a maximum of 80 mm (Fig. 6). Further, the mean quasigeoid error in the final model is approximately 2 mm less than that of the EGM2008 quasigeoid. This is commensurate with the increased precision seen in the comparison with GNSS-levelling data (Fig. 2).

The error variances of the G_1 terms have been propagated independently through Stokes’s integral to assess their contribution to the uncertainty (i.e. evaluating the second term in Eq. (11) with the G_1 term error variances in place of the full Molodensky anomaly variances). The standard deviation of these values (i.e. square root of the second term of Eq. 11) is shown in Fig. 7. On comparison with Fig. 6b, onshore, the G_1 terms contribute greatly to the uncertainty signal. They account for at least half of the total error, having a maximum value of 27 mm in the South East of Australia. This demonstrates that for a robust uncertainty estimate of the quasigeoid derived using the Molodensky anomaly, the contribution of the G_1 terms should not be overlooked.

5 Concluding remarks

We have presented a $1'' \times 1''$ grid of first-order Molodensky G_1 terms and a grid of corresponding uncertainty estimates for the entire Australian continent. This work closes a gap in the existing literature on the methodology to compute uncertainty estimates for the G_1 term. The formulas allow for DEM and gravity anomaly uncertainty estimates to be propagated through the convolution integrals and subsequently into the quasigeoid model.

We combined the G_1 terms with an existing grid of free air anomalies to produce Molodensky gravity anomalies. These were used to compute quasigeoid models by the remove—compute—restore procedure with EGM2008 as the reference field. As was the case for AGQG2017 (Featherstone et al. 2018a), the solution that agreed closest with ~7000 GPS-levelling data was given by an integration cap radius of 0.5° and a modification degree of 40. The Molodensky quasigeoid solutions appear to be less precise than the Faye ones. Our preliminary tests appear to indicate that this is attributable to the mismatch between the spatial resolution of the gravity data and DEM. For the currently available gravity and DEM data covering Australia, it appears that planar terrain corrections are preferable to Molodensky G_1 terms.

We combined the G_1 term uncertainty estimates with existing grid of free air anomaly uncertainty estimates and propagated the resulting grid through the modified Stokes’s integral. The Molodensky gravity anomaly uncertainties with mean a of 2 mGal and a maximum of 54 mGal translate into quasigeoid height uncertainties with a mean of 4 mm and a maximum of 80 mm. The largest uncertainty values were found in the South East where the topography varies most

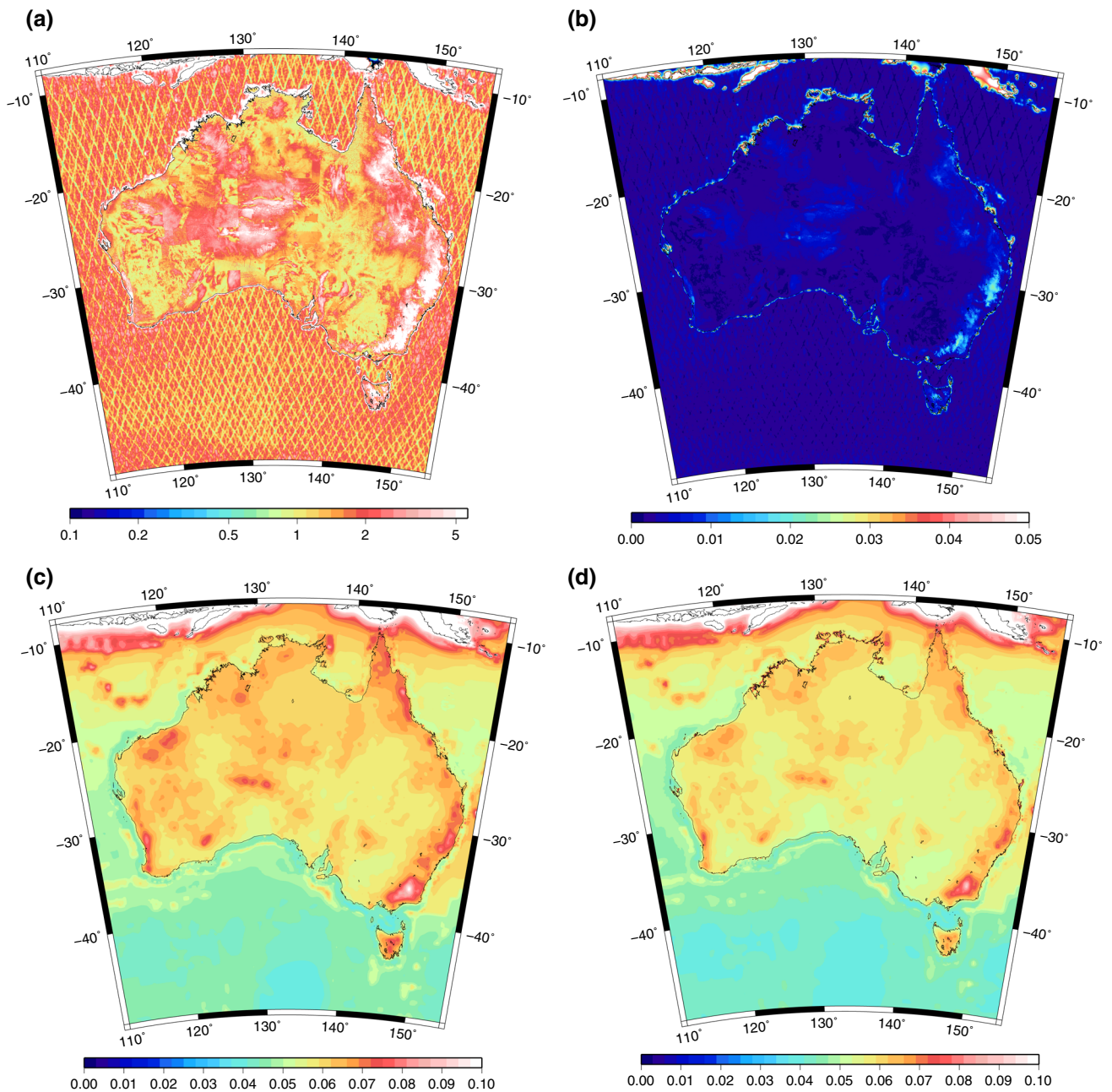


Fig. 6 a The Molodensky gravity anomaly error standard deviation [min: 0.003 max: 54.201 mean: 2.001 STD: 2.880] mGal. **b** Stokes's integral error propagation (i.e. second term in Eq. 11) of the Molodensky gravity anomaly error data evaluated with FEO modification degree of 40 and integration cap radius of 0.5° [min: 0.000 max: 0.080: mean:

0.004 STD: 0.006] m. **c** The EGM2008 quasigeoid height errors standard deviation [min: 0.038 max: 0.299 mean: 0.057 STD: 0.019] m. **d** The quasigeoid height standard deviation [min: 0.038 max: 0.270 mean: 0.055 STD: 0.017] m

strongly. These precision estimates generally agree with what is anticipated of the quasigeoid accuracy in those areas.

Finally, it is important to recall that the derivation of the G_1 term uncertainties given here is based on the assumption that the DEM and free air anomaly errors are zero-mean Gaussian random variables and are spatially independent.

Refining these assumptions and modifying the error propagation formula may well improve the precision of the derived uncertainty values but could ultimately be costly in terms of their numerical evaluation.

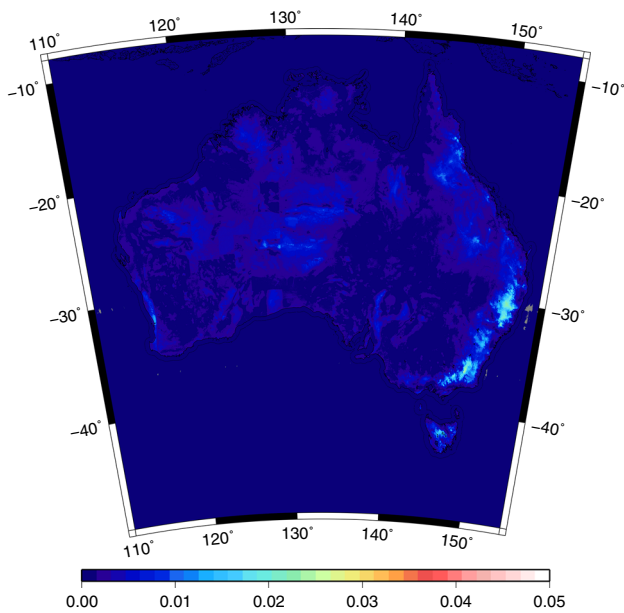


Fig. 7 Stokes's integral error propagation of the Molodensky G_1 term standard deviation [min: 0 max: 0.027 mean: 0.001 STD: 0.002] m

Acknowledgements This work has been supported financially by the Cooperative Research Centre for Spatial Information, whose activities are funded by the Business Cooperative Research Centres Programme and by Geoscience Australia. Maps in this paper were produced using GMT (Wessel et al. 2013). Jack McCubbine and Nicholas Brown publish this paper with the permission of the Chief Executive Officer of Geoscience Australia. We would like to thank the editors and the anonymous reviewers for their useful suggestions to improve this manuscript.

Open Access This article is distributed under the terms of the Creative Commons Attribution 4.0 International License (<http://creativecommons.org/licenses/by/4.0/>), which permits unrestricted use, distribution, and reproduction in any medium, provided you give appropriate credit to the original author(s) and the source, provide a link to the Creative Commons license, and indicate if changes were made.

Appendix A: DEM and gravity anomaly correlated uncertainties

The “topographic restoration procedure” (Featherstone and Kirby 2000) was developed to reduce aliasing the gravitational effect of topography when interpolating gravity anomalies. Bouguer gravity anomalies are generally smoother than free air gravity anomalies and so are better suited to interpolation. First, pointwise simple Bouguer gravity anomalies are interpolated onto a regular grid, and then the gravitational effect of a slab of topography is restored to the gridded gravity signal at each grid node by a reverse Bouguer slab correction from a DEM. The reverse Bouguer slab correction is determined by multiplying DEM gridded heights by a factor of 0.0419ρ , where $\rho = 2670 \text{ kg/m}^3$ is the assumed-constant topographic bulk density.

The topographic restoration procedure is expected to generate more reliable mean free air gravity anomalies than directly interpolating pointwise free air gravity anomalies. However, it implicitly causes errors in the DEM and the gridded gravity anomalies to become correlated. This is contradictory to the assumption (iii) used for the derivation in Sect. 3 and necessitates a reformulation of Eq. (9).

The free air gravity anomaly is instead given by Eq. (A1) below, where Δg_{BA} is the simple Bouguer gravity anomaly, and the variance of the Molodensky gravity anomaly is given by Eq. (A2).

$$\Delta g_{FA} = \Delta g_{BA} + 0.111H^* \quad (\text{A1})$$

$$\text{Var}(\Delta g) = \text{Var}(\Delta g_{BA}) + \text{Var}(0.111H^* + G_1) \quad (\text{A2})$$

As before, a small change in the gridded data set can be evaluated by looking at the complete Taylor series expansion of $(0.111H^* + G_1)$ for a single grid element

$$\begin{aligned} & 0.111(H^* + dH^*) + G'_1(H'^* + dH'^*, H^* + dH^*, \Delta g'_{BA} \\ & \quad + d\Delta g'_{BA}) - 0.111H^* - G'_1(H'^*, H^*, \Delta \widehat{g}_{BA}) \\ & = 0.111dH^* + \frac{\Delta\phi\Delta\lambda}{2\pi I^3} [dH'^*(\Delta g'_{BA} + 0.222H'^* \\ & \quad - 0.111H^*) - dH^*(\Delta g'_{BA} + 0.111H'^*) \\ & \quad + d\Delta g'_{BA}(H'^* - H^*) + 0.111dH'^{*2} - 0.111dH^*dH'^* \\ & \quad + dH'^*d\Delta g'_{BA} - dH^*d\Delta g'_{BA}] \quad (\text{A3}) \end{aligned}$$

Under the assumption of uncorrelated errors among the cells of the gridded data, the variance of the “reconstructed” Molodensky gravity anomaly is

$$\begin{aligned} \text{Var}(\Delta g) = & \sigma_{\Delta g_{BA}}^2 + 0.111^2\sigma_{dH^*}^2 + \frac{\Delta\phi^2\Delta\lambda^2}{4\pi^2} \\ & \left[\left(\left[\Delta g_{BA}^2 + 0.222^2H'^{*2} + 0.444\Delta g'_{BA}H'^* \right] \sigma_{dH'^*}^2 \right) \right. \\ & \quad * \frac{1}{16} - 2 * 0.111 * H^* \left(\left[0.222H'^* + \Delta g'_{BA} \right] \sigma_{dH'^*}^2 * \frac{1}{16} \right) \\ & \quad + 0.111^2 H^{*2} \left(\sigma_{dH'^*}^2 * \frac{1}{16} \right) \\ & \quad + \sigma_{dH^*}^2 \left(\left(\Delta g'_{BA} + 0.111H'^* \right)^2 * \frac{1}{16} \right) + \left(H'^{*2} \sigma_{d\Delta g'_{FA}}^2 * \frac{1}{16} \right) \\ & \quad - 2H^* \left(\sigma_{d\Delta g'_{FA}}^2 H' * \frac{1}{16} \right) + H^{*2} \left(\sigma_{d\Delta g'_{FA}}^2 * \frac{1}{16} \right) \\ & \quad + 0.111^2 \left(2 \left(\sigma_{dH^*}^2 \right)^2 * \frac{1}{16} \right) + 0.111^2 \sigma_{dH^*}^2 \left(\sigma_{dH'^*}^2 * \frac{1}{16} \right) \\ & \quad \left. + \left(\sigma_{dH'^*}^2 \sigma_{d\Delta g'_{FA}}^2 \right) * \frac{1}{16} + \sigma_{dH^*}^2 \left(\sigma_{d\Delta g'_{FA}}^2 * \frac{1}{16} \right) \right] \\ & - 2 * 0.111 * \frac{\Delta\phi\Delta\lambda}{2\pi} \sigma_{dH^*}^2 \left(\left(\Delta g'_{BA} + 0.111H'^* \right) * \frac{1}{16} \right) \quad (\text{A4}) \end{aligned}$$

Equation (A4) is significantly more complicated to compute than Eq. (8) and requires substantially more computational steps. However, if one chooses to use the topographic

restoration procedure (Featherstone and Kirby 2000), Eq. (A4)-derived uncertainty estimates should be more realistic compared to using Eq. (9).

References

- Amod A, Merry CL (2002) A note on the Molodensky G_1 term. *Int Geoid Serv Bull* 12:62–80
- Banz L, Costea A, Gimperlein H, Stephan EP (2014) Numerical simulations for the non-linear Molodensky problem. *Stud Geophys Geod* 58(4):489–504. <https://doi.org/10.1007/s11200-013-0141-2>
- Baussus-von Luetzow H (1971) New solution for the anomalous gravity potential. *J Geophys Res* 76(20):4884–4891. <https://doi.org/10.1029/JB076i020p04884>
- Brovar VV (1964) On the solutions of Molodensky's boundary value problem. *Bull Géod* 38(2):167–173. <https://doi.org/10.1007/BF02526971>
- Burša M (1965) On practical application of the solution of Molodensky's integral equation in the first approximation. *Stud Geophys Geod* 9(2):144–150. <https://doi.org/10.1007/BF02607323>
- Costea A, Gimperlein H, Stephan EP (2014) A Nash–Hörmander iteration and boundary elements for the Molodensky problem. *Numer Math* 127(1):1–34. <https://doi.org/10.1007/s00211-013-0579-8>
- Denker H, Tziavos IN (1999) Investigation of the Molodensky series terms for terrain reduced gravity field data. *Bollettino di Geofisica Teorica ed Applicata* 40(3–4):195–203
- Featherstone WE, Filmer MS (2012) The north–south tilt in the Australian height datum is explained by the ocean's mean dynamic topography. *J Geophys Res Oceans* 117(C8):C08035. <https://doi.org/10.1029/2012JC009774>
- Featherstone WE, Kirby JF (2000) The reduction of aliasing in gravity anomalies and geoid heights using digital terrain data. *Geophys J Int* 141(1):204–212. <https://doi.org/10.1046/j.1365-246X.2000.0082.x>
- Featherstone WE, Evans JD, Olliver JG (1998) A Meissl-modified Vanicek and Kleusberg kernel to reduce the truncation error in gravimetric geoid computations. *J Geod* 72(3):154–160. <https://doi.org/10.1007/s001900050157>
- Featherstone WE, McCubbin JC, Brown NJ, Claessens SJ, Filmer MS, Kirby JF (2018a) The first Australian gravimetric quasigeoid model with location-specific uncertainty estimates. *J Geod* 92(2):149–168. <https://doi.org/10.1007/s00190-017-1053-7>
- Featherstone WE, Brown NJ, McCubbin JC, Filmer MS (2018b) Description and release of Australian gravity field model testing data. *Australian Journal of Earth Sciences* 65(1):1–7. <https://doi.org/10.1080/08120099.2018.1412353>
- Foroughi I, Tenzer R (2014) Assessment of the direct inversion scheme for the quasigeoid modeling based on applying the Levenberg–Marquardt algorithm. *Appl Geomat* 6(3):171–180. <https://doi.org/10.1007/s12518-014-0131-2>
- Freedon W, Mayer C (2006) Multiscale solution for the Molodensky problem on regular telluroidal surfaces. *Acta Geod Geophys Hung* 41(1):55–86. <https://doi.org/10.1556/AGeod.41.2006.1.6>
- Frigo M, Johnson SG (2005) The design and implementation of FFTW3. *Proc IEEE* 93(2):216–231. <https://doi.org/10.1109/JPR OC.2004.840301>
- Gallant JC, Dowling TI, Read AM, Wilson N, Tickle P, Inskip C (2011) 1 second SRTM derived digital elevation models user guide. Geoscience Australia www.ga.gov.au/topographic-mapping/digital-elevation-data.html. http://www.ga.gov.au/metadata-gateway/metadata/record/gcat_72759. Accessed 16 Jan 2016
- Heiskanen WA, Moritz H (1967) *Physical geodesy*. Freeman, San Francisco, p 264
- Hirt C, Featherstone WE, Claessens SJ (2011) On the accurate numerical evaluation of geodetic convolution integrals. *J Geod* 85(8):519–538. <https://doi.org/10.1007/s00190-011-0451-5>
- Hutchinson MF (1989) A new procedure for gridding elevation and stream line data with automatic removal of spurious pits. *J Hydrol* 106(3–4):211–232. [https://doi.org/10.1016/0022-1694\(89\)90073-5](https://doi.org/10.1016/0022-1694(89)90073-5)
- Lemoine FG, Kenyon SC, Factor JK, Trimmer RG, Pavlis NK, Chinn DS, Cox CM, Klosko SM, Luthcke SB, Torrence MH, Wang YM, Williamson RG, Pavlis EC, Rapp RH, Olson TR (1998) The development of the joint NASA GSFC and the National Imagery and Mapping Agency (NIMA) geopotential model EGM96, NASA/TP-1998-206861. Natl Aeronaut Space Adm, USA
- Li YC, Sideris MG, Schwarz K-P (1995) A numerical investigation on height anomaly prediction in mountainous areas. *Bull Géod* 69(3):143–156. <https://doi.org/10.1007/BF00815483>
- McCubbin JC, Featherstone WE, Kirby JF (2017) Fast Fourier-based error propagation for the gravimetric terrain correction. *Geophysics* 82(4):G71–G76. <https://doi.org/10.1190/geo2016-0627.1>
- Merry CL (2003) DEM-induced errors in developing a quasi-geoid model for Africa. *J Geodesy* 77(9):537–542. <https://doi.org/10.1007/s00190-003-0353-2>
- Mojžeš M, Janák J, Papčo J (2005) Improvement of the gravimetric model of quasigeoid in Slovakia. *Newton's Bull* 3:27–31
- Molodensky MS, Yeremeyev VF, Yurkina MI (1960) Methods for study of the external gravitational field and figure of the earth. TRUDY Ts NIIGAIK, 131, Geodezizdat, Moscow (English transl.: Israel Program for Scientific Translation, Jerusalem 1962)
- Molodensky MS, Yeremeyev VF, Yurkina MI (1962) An evaluation of accuracy of Stokes's series and of some attempts to improve his theory. *Bull Géod* 36(1):19–37. <https://doi.org/10.1007/BF02528170>
- Moritz H (1968) On the use of the terrain correction in solving Molodensky's problem. Report 108, Department of Geodetic Science and Surveying, Ohio State University, Columbus, USA
- Moritz H (1970) A new series solution of Molodensky's problem. *Bull Géod* 44(2):183–195. <https://doi.org/10.1007/BF02521707>
- Moritz H (2015) *Classical physical geodesy*. Handbook of Geomatics, second edition edn. Springer, Heidelberg, pp 253–289. https://doi.org/10.1007/978-3-642-54551-1_6
- Pavlis NK, Saleh J (2005) Error propagation with geographic specificity for very high degree geopotential models. In: *Gravity, geoid and space missions*. Springer, Berlin, pp 149–154
- Pavlis NK, Holmes SA, Kenyon SC, Factor JK (2012) The development and evaluation of the Earth Gravitational Model 2008 (EGM2008). *J Geophys Res Solid Earth* 117(B4):B04406. <https://doi.org/10.1029/2011JB008916>
- Pavlis NK, Holmes SA, Kenyon SC, Factor JK (2013) Correction to : The development and evaluation of the Earth Gravitational Model 2008 (EGM2008). *J Geophys Res Solid Earth* 118(5):2633. <https://doi.org/10.1029/jgrb.50167>
- Pellinen LP (1962) Accounting for topography in the calculation of quasigeoidal heights and plumb-line deflections from gravity anomalies. *Bull Géod* 36(1):57–65. <https://doi.org/10.1007/BF02528175>
- Rapp RH (1975) Effect of certain anomaly correction terms on potential coefficient determinations of the Earth's gravitational field. *Bull Géod* 49(1):57–63. <https://doi.org/10.1007/BF02523943>
- Sandwell DT, Garcia E, Soofi K, Wessel P, Smith WHF (2013) Towards 1 mGal global marine gravity from CryoSat-2, Envisat, and Jason-1. *Lead Edge* 32(8):892–899. <https://doi.org/10.1190/tle3208089.2.1>

- Sansó F (1978) Molodensky's problem in gravity space: a review of the first results. *Bull Géod* 52(1):59–70. <https://doi.org/10.1007/BF02521792>
- Sansó F (1989) New estimates for the solution of Molodensky's problem. *Manuscr Geod* 14(2):68–76
- Sideris MG, Schwarz KP (1986) Solving Molodensky's series by fast Fourier transform techniques. *Bull Géod* 60(1):51–63. <https://doi.org/10.1007/BF02519354>
- Sideris MG, Schwarz KP (1988) Advances in the numerical solution of the linear Molodensky problem. *Bull Géod* 62(1):59–70. <https://doi.org/10.1007/BF02519325>
- Vaniček P (1974) Brief outline of the Molodensky theory. Lecture Notes 23, Department of Geodesy and Geomatics Engineering, University of New Brunswick, Fredericton, Canada. <http://www2.unb.ca/gge/Pubs/LN23.pdf>
- Vaniček P, Featherstone WE (1998) Performance of three types of Stokes's kernel in the combined solution for the geoid. *J Geod* 72(12):684–697. <https://doi.org/10.1007/s001900050209>
- Wessel P, Smith WHF, Scharroo R, Luis JF, Wobbe F (2013) Generic mapping tools: improved version released. *EOS Trans AGU* 94(45):409–410. <https://doi.org/10.1002/2013EO450001>
- Yu J-H, Zhu Z-W, Peng F-Q (2001) Wavelet arithmetic of G_1 -term in Molodensky's boundary value problem. *Acta Geophys Sin* 44(1):119–127. <https://doi.org/10.1002/cjg2.121>